JACS
JOURNAL OF THE AMERICAN CHEMICAL SOCIETY

Article

pubs.acs.org/JACS

Direct DNA Analysis with Paper-Based Ion Concentration Polarization

Max M. Gong,[†] Reza Nosrati,[†] Maria C. San Gabriel,[‡] Armand Zini,[‡] and David Sinton*[,†]

[†]Department of Mechanical and Industrial Engineering, University of Toronto, 5 King's College Rd., Toronto, Ontario, Canada M5S 3G8

[‡]Urology Research Laboratory, Department of Surgery, Royal Victoria Hospital, McGill University, Montreal, Quebec, Canada H4A 3J1

Supporting Information

ABSTRACT: DNA analysis is essential for diagnosis and monitoring of many diseases. Conventional DNA testing is generally limited to the laboratory. Increasing access to relevant technologies can improve patient care and outcomes in both developed and developing regions. Here, we demonstrate direct DNA analysis in paper-based devices, uniquely enabled by ion concentration polarization at the interface of patterned nanoporous membranes in paper (paper-based ICP). Hepatitis B virus DNA targets in human serum are simultaneously preconcentrated, separated, and detected in a single 10 min operation. A limit of detection of 150 copies/mL is achieved without prior viral load amplification, sufficient for early diagnosis of hepatitis B. We clinically assess the DNA integrity of sperm cells in raw human semen samples. The percent DNA fragmentation results from the paper-based ICP devices strongly correlate (R^2 = 0.98) with the sperm chromatin structure assay. In all cases, agreement was 100% with respect to the clinical decision. Paper-based ICP can provide inexpensive and accessible advanced molecular diagnostics.

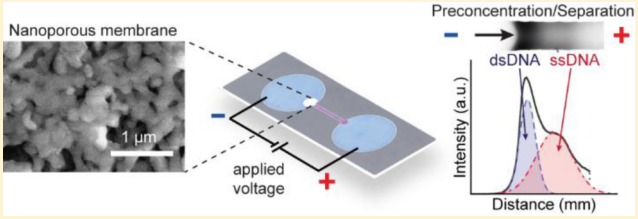

INTRODUCTION

DNA analysis is fundamental to forensic science,[1] genetics,[2] and disease diagnosis.[3] Conventional DNA testing relies on methods generally limited to the laboratory. For example, the polymerase chain reaction (PCR) is the most commonly used method for viral load detection.[3] Similarly, the flow cytometry-based sperm chromatin structure assay (SCSA) is the gold standard for sperm DNA integrity assessment.[4] Nanotechnology and, specifically, nanostructured sensors show potential for scalable analysis of DNA.[5] Common classes of these sensors include nanopores,[6,7] plasmonic nanohole arrays,[8] single and arrayed nanoparticles,[9−11] nanostructured microelectrodes,[12,13] and nanowires.[14,15] These nanostructures have also been integrated into microfluidic and nanofluidic systems,[5] with demonstrated performance comparable to conventional DNA testing technologies. In all of these cases, however, the nanofabrication in silicon and glass is a barrier to widespread application.

Paper has emerged as an inexpensive, versatile, and scalable platform for diagnostics, with microfluidic paper-based analytical devices (μPADs) as a central format.[16−18] Recent advances in μPADs position these technologies for broad diagnostic application.[19−22] Specifically, the integration of nanomaterials into paper potentially offers enhanced detection capabilities.[23] Nanoparticles are the most commonly employed nanomaterial in lateral flow assays and μPADs, and are mainly used as labels for colorimetric detection of DNA and other analytes.[23] The plasmonic properties of these particles have also been exploited for label-free sensing in paper.[24−26] Moreover, graphene nanosheets have been used for electrochemical sensing in paper-based devices.[27] The nanomaterials in these applications are mainly used as static sensing elements. Leveraging nanomaterials for active transport in paper would enable advanced control of target analytes, extending the current molecular diagnostic capabilities of paper-based devices.

Here, we demonstrate direct DNA analysis in paper-based devices, uniquely enabled by ion concentration polarization (ICP) effects at the interface of patterned nanoporous membranes in paper (herein referred to as paper-based ICP). ICP is an electrokinetic phenomenon caused by transport of ions through ion-selective nanostructures.[28] It has been applied to water desalination[29,30] and biomolecular concentration in microchannels.[31] Other electrokinetic phenomena, such as isotachophoresis[32−35] and electrophoresis,[36−38] have been demonstrated in paper-based devices. We apply our paper-based ICP approach to detect hepatitis B and assess male fertility. Hepatitis B virus (HBV) DNA targets in human serum are simultaneously preconcentrated, separated, and detected in a single operation with a limit of detection (LOD) of 150 copies/mL. This LOD is achieved without prior PCR amplification of viral load, eliminating the need for thermal cycling. We clinically assess the DNA integrity of sperm cells in raw human semen samples by preconcentrating and separating

Received: August 12, 2015
Published: October 8, 2015

DOI: 10.1021/jacs.5b08523
J. Am. Chem. Soc. 2015, 137, 13913−13919

denatured DNA from intact DNA. The percent DNA fragmentation results from the paper-based ICP devices strongly correlate (R^2 = 0.98) with the conventional sperm chromatin structure assay (SCSA) and inform the same clinical outcomes.

EXPERIMENTAL SECTION

Design and Operation of the Paper-Based ICP Device. The paper-based ICP device is nitrocellulose paper with a sample channel and reservoirs defined by patterned wax, and a region coated with cation-selective nanoporous Nafion (Figure 1a). Nitrocellulose paper

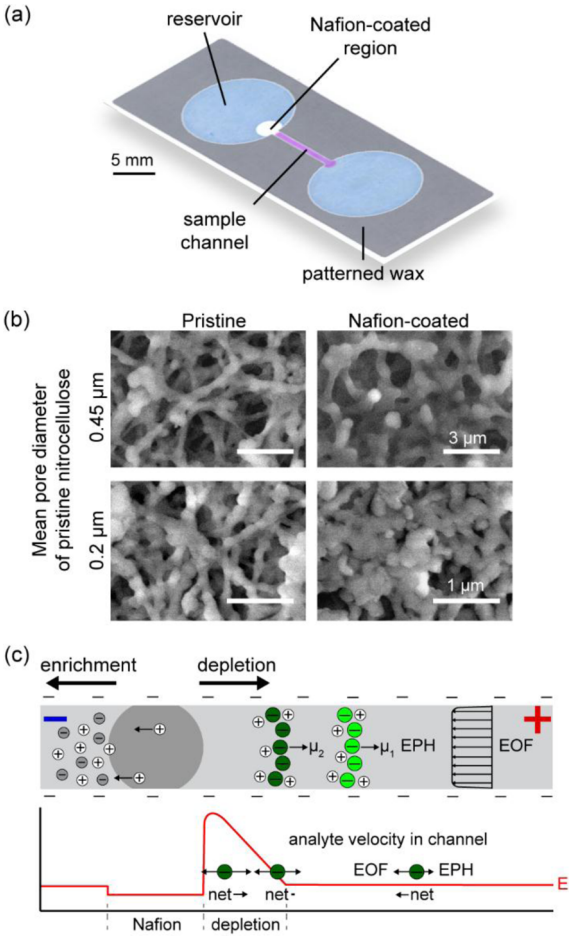

Figure 1. Design and operation of the paper-based ICP device. (a) Device schematic with reservoirs (blue), sample channel (purple), and Nafion-coated region (white). (b) Environmental scanning electron microscopy images of nitrocellulose paper with and without Nafion coating. (c) Schematic of ICP enrichment and depletion effects under applied voltage. Net movement of analytes is governed by electrophoretic migration (EPH) and electroosmotic flow (EOF), in response to the local electric field strength, *E*.

is used as the substrate for several reasons: (1) it is widely used for the analysis of biomolecules (e.g., protein and nucleic acid blotting),[39] (2) it is the most commonly used substrate for commercial lateral flow assays and μPADs,[39] and (3) it has been demonstrated as a suitable substrate for electrokinetic operations.[32] Nanoporous Nafion is the main functional component in the device enabling nanoscale electrokinetic transport of ions for inducing ICP. Nafion-coated regions of nitrocellulose paper with original mean pore diameters of 0.2 and 0.45 μm are shown in environmental scanning electron microscopy images in Figure 1b.

Device designs were created in Microsoft PowerPoint and printed on nitrocellulose paper (mean pore diameters of 0.2 and 0.45 μm, Bio-Rad Laboratories Ltd., Canada) using a solid wax printer (ColorQube 8570N, Xerox Canada, Canada). Printed devices were heated in an oven at 150 °C for 5 min to allow the wax to penetrate through the thickness of the nitrocellulose paper. Nafion perfluorinated resin solution (20% wt in lower aliphatic alcohols and water, Sigma-Aldrich) was manually pipetted into each device, 0.5 μL of Nafion per device. Following this step, devices were immersed in deionized (DI) water for 30 min to hydrate the Nafion. Fabricated devices were covered in Petri dishes at room temperature until use. For the Nafion concentration experiments in Figure 2e, the 20% wt stock solution was diluted to concentrations of 5% wt, 10% wt, and 15% wt using a solution of DI water (4 parts), *n*-propanol (5 parts), and ethanol (1 part) (from MSDS). Concentrations higher than 20% wt were attempted with Nafion perfluorinated resin powder (Sigma-Aldrich) prepared in the diluting solution; however, Nafion precipitated out of solution at these concentrations.

To operate the device, reservoirs are prewetted with DI water, and sample is added to the sample channel. A voltage is applied to induce ICP (Figure 1c). Cations selectively migrate through the Nafion-coated region toward the cathode (i.e., negatively charged electrode) causing an ion enrichment zone at the cathodic Nafion interface. This efflux of cations causes anions to vacate the region due to electrical neutrality, forming an ion depletion zone. The depletion zone propagates and repels anions toward the anode (i.e., positively charged electrode). The net movement of anions in the channel is ultimately dictated by electrophoretic migration (EPH) toward the anode and electroosmotic flow (EOF) toward the cathode. Anions experience different electrokinetic forces along the channel as a result of local changes to the applied electric field and ionic concentration from ICP.[40] Specifically, lower ionic concentrations lead to higher EOF transport rates and vice versa.[41] EOF is dominant downstream of the depletion zone, causing net movement of analytes toward the depletion boundary in the cathodic direction. EPH is higher than EOF in the depletion zone, causing anions to migrate toward the depletion boundary in the anodic direction. The balance of these two opposing effects focuses ions at the depletion boundary. For a system with multiple anionic analytes, each analyte migrates at a different net velocity due to variations in their electrophoretic mobility, enabling separation following preconcentration.

Preparation of Fluorescent Tracers and Biological Samples. Fluorescein and calcein were used as fluorescent tracers and were both acquired from Sigma-Aldrich. Stock solutions of fluorescein and calcein were prepared using DI water, with final molar concentrations of 2 and 1 μM, respectively. The pH values of the solutions were adjusted to 8.0 using 5 M HCl and 1 M NaOH solutions. Testing solution was prepared by mixing equal volumes of fluorescein and calcein solutions with a final molar concentration ratio of 2:1.

A Low Mass DNA ladder (117.5 ng/μL stock solution, Thermo Fisher Scientific Inc.) was used to demonstrate DNA separation in the device. The DNA ladder was stained with 1× Quant-iT PicoGreen dsDNA Reagent (200× stock solution diluted as per supplier instructions, Thermo Fisher Scientific Inc.) at a volume ratio of 1:20 (DNA:PicoGreen) and incubated at room temperature for 5 min.

Hepatitis B analysis used synthetic hepatitis B virus (HBV) DNA (6.8×10^8 copies/mL stock solution, ATCC VR3232SD) obtained from Cedarlane, Canada. Stock solution contained fragments from the precore, core, polymerase, surface, and X regions of the viral genome, as specified by the manufacturer. Two separate dilution series were made from the stock HBV DNA using DNase/RNase-free distilled water (Thermo Fisher Scientific Inc.) and human serum (final serum protein concentration of 3 mg/mL, Cedarlane, Canada). Final sample concentrations ranged from 10 to 10^8 copies/mL at 10-fold intervals. Each sample was stained with 1× PicoGreen at a volume ratio of 1:20 (DNA:PicoGreen) and incubated at room temperature for 5 min.

Human semen samples from patients and healthy donors (n = 7) were obtained by masturbation after 2–4 days of sexual abstinence at the Urology Research Laboratory, Royal Victoria Hospital, Canada. All donors signed an informed consent, and the information for this study

DOI: 10.1021/jacs.5b08523
J. Am. Chem. Soc. 2015, 137, 13913–13919

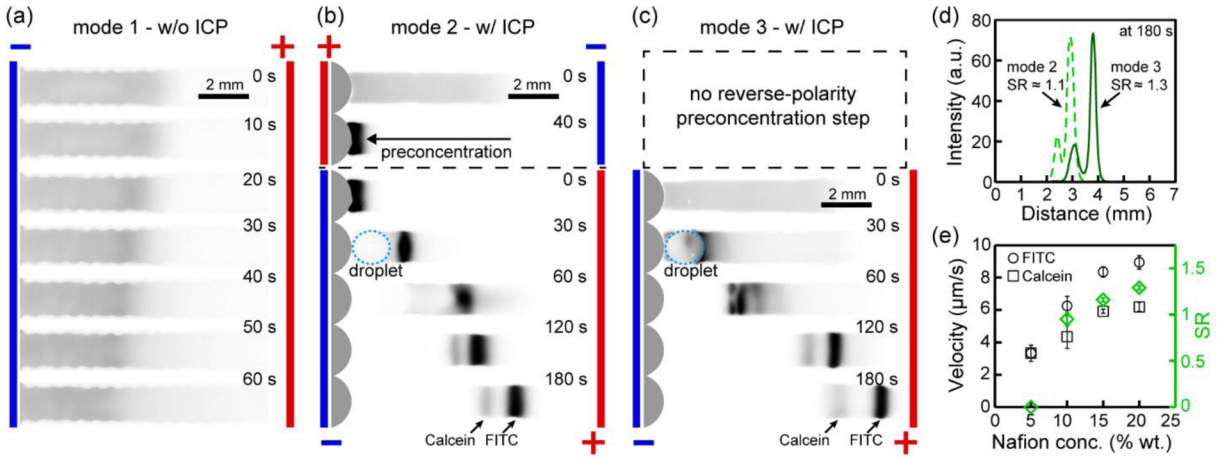

Figure 2. Preconcentration and separation in the paper-based ICP device. (a) Operating mode 1—transport without ICP. (b) Operating mode 2—preconcentration and separation with switching-polarity ICP. (c) Operating mode 3—direct preconcentration and separation with ICP. (d) Separation resolution (SR) in modes 2 and 3. (e) Effect of Nafion concentration (% wt.) on the separation process. Data points are the average of n = 3 measurements with error bars as one standard deviation. Images have been contrast adjusted for presentation (similarly in each case).

remains confidential within the institution. Samples were incubated at 37 °C for 30 min to allow liquefaction. Computer-assisted sperm analysis (CASA) was used to obtain standard semen parameters in accordance with World Health Organization guidelines. Semen samples were diluted to a concentration of 20 million sperm cells per milliliter (M/ml) with HBS buffer (135 mM NaCl, 25 mM HEPES, 5 mM KCl, 0.75 mM $Na_2HPO_4{\cdot}2H_2O$, 12 mM Glucose, pH 7.4).

To lyse the sperm cells, a 10 μL aliquot of the diluted sample was treated with 40 μL of 50 mM dithiothreitol (DTT), 50 μL of distilled water, and 300 μL of 8 M GuHCl in separate steps. The solution was vortexed for 30 s between each step and for 15 s after the final step. Lysed DNA was stained with 1× SYBR Green I (10000× stock solution diluted as per supplier instructions, Thermo Fisher Scientific Inc.) at a volume ratio of 1:1 (DNA:SYBR Green) and incubated at room temperature for 10 min. The resulting solution was diluted 500-fold in DI water and used immediately.

Sperm Chromatin Structure Assay. Raw semen samples were diluted to a concentration of 10 M/mL in TNE buffer (0.1 M TRIS buffer, 0.15 M NaCl, 1 mM EDTA, pH 7.4). After dilution, 200 μL of the sample was treated with 400 μL acid detergent solution (0.08 M HCl, 0.15 M NaCl, 0.1% Triton X-100, pH 1.2) for 30 s. After 30 s, 1.2 mL of staining buffer (6 μg/mL acridine orange, 37 mM citric acid, 126 mM Na_2HPO_4, 1 mM disodium EDTA, 0.15 M NaCl, pH 6.0) was admixed to the test tube. The sample was placed into the MACSQuant Analyzer (Miltenyi Biotec, Bergisch Gladbach, Germany) equipped with a 488 nm air-cooled laser with the sample flowing to establish sheath/sample flow. Measurements were taken after 3 min of staining. A minimum of 5000 cells from two aliquots of each sample were analyzed at a flow rate of 100–200 events/sec by FACS scan interfaced with a data handler (CELLQUEST 3.1, Becton Dickinson) on a Power Macintosh 7600/132 computer (Cupertino, CA). WinList (Verity Softwarehouse Inc., Topsham, ME) was used to generate the cytogram (red vs green fluorescence) and histogram (total cells vs % DFI) plots, as well as % DFI readings. A mean of the two sperm % DFI values was reported. The variability of the replicate SCSA measures (% DFI) is less than 5%.

Data Acquisition and Analysis. For the characterization and HBV DNA experiments, an inverted fluorescence microscope (DMI 6000B, Leica Microsystems Inc., Canada) was used to visualize fluorescent tracers and stained HBV DNA with a L5 filter cube. Image sequences were captured using a CCD camera (Orca-AG, Hamamatsu Photonics K. K.). For the sperm DNA integrity experiments, an upright fluorescence microscope (Axiophot, Carl Zeiss AG, Germany) was used to visualize stained sperm DNA with a green fluorescence filter. Image sequences were captured using a CCD camera equipped with the microscope. All captured images were processed in ImageJ and Adobe Photoshop. Data quantification was completed in Microsoft Excel and Mathematica.

RESULTS AND DISCUSSION

Preconcentration and Separation in the Paper-Based ICP Device. We demonstrated three different operating modes using anionic fluorescent tracers [fluorescein isothiocyanate (FITC), 332.3 g/mol; calcein, 622.6 g/mol] as model analytes: (1) transport without ICP; (2) preconcentration and separation with switching-polarity ICP; and (3) direct preconcentration and separation with ICP. FITC and calcein were chosen as model analytes for the experiments in Figures 2 and 3 because they are negatively charged and are inherently fluorescent, making them suitable for modeling DNA transport in the device. The two tracers are also potentially useful for modeling other anionic biomolecules, including RNA and proteins. For transport in the absence of ICP (mode 1), EOF was dominant over EPH everywhere, resulting in net migration of analytes toward the cathode with no preconcentration or separation effects (Figure 2a and Movie 1).

For preconcentration and separation with switching-polarity ICP (mode 2), a Nafion-coated region is employed to achieve both enrichment and depletion (Figure 2b). Specifically, ICP applied with the anode on the left preconcentrated anions at the Nafion interface via enrichment ($t \leq 40$ s). Switching the polarity of the electrodes caused depletion to grow at the same interface, transporting and separating the preconcentrated analytes left-to-right (Movie 2). In this mode, a droplet of bulk (nonfluorescent) fluid grew on the surface of the paper near the Nafion interface. This accumulation of bulk fluid is a result of a mismatch between EOF transport rates through the paper and the Nafion-coated region.

For direct preconcentration and separation with ICP (mode 3), no reverse-polarity preconcentration step was employed, and ICP was applied only in the forward direction (Figure 2c and Movie 3). Analytes rapidly collected at the depletion boundary ($t \leq$ 30s) as a result of strong initial EOF (to the left), achieving early preconcentration without a reverse polarity. EOF was reduced as the electrically insulating depletion zone grew, and the analytes were electrophoretically separated left-to-right. It is noteworthy that as the depletion boundary grows, the reduction in the electric field strength

DOI: 10.1021/jacs.5b08523
J. Am. Chem. Soc. 2015, 137, 13913–13919

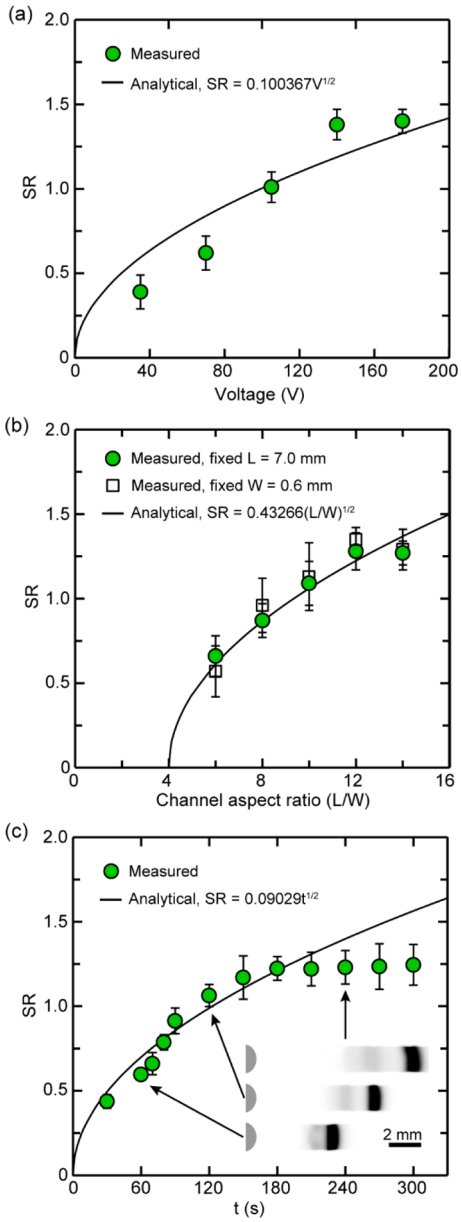

Figure 3. Characterization of separation parameters for the paper-based ICP device. (a) Separation resolution (SR) as a function of applied voltage, using devices of fixed geometry (channel length of 7 mm and width of 0.6 mm). (b) SR as a function of channel aspect ratio (i.e., length/width), with a fixed field strength of 200 V/cm. (c) SR as a function of residence time, using an applied field of 200 V/cm and devices with channel aspect ratio of 12. SR improves with increasing residence time up to 180 s, where band broadening from Joule heating becomes limiting (inset images). Plotted points are the average of n = 3 measurements with error bars as one standard deviation. Images have been contrast-adjusted for presentation.

reduces both EOF and EPH (electric field diagram in Figure 1c); however, EOF is additionally reduced by the increasing ionic concentration ahead of the depletion zone. Although the underlying electrokinetic phenomena are complex, the paper-based ICP approach is robust and easy to use.

Characterization of the Separation Process. The separation quality achieved in modes 2 and 3 was quantified by a separation resolution (SR) metric, which is defined as the ratio of peak-to-peak distance between adjacent bands to their average width.[42] SR values were comparable at ~1.1 for mode 2 and ~1.3 for mode 3, indicating that the reverse-polarity preconcentration step in mode 2 is not advantageous nor necessary (Figure 2d). We also investigated the effect of Nafion concentration (% wt) on the separation process (Figure 2e). Cation transport increased with Nafion concentration, resulting in stronger ICP effects.[43] No separation of the analytes was detectable for 5% wt. Nafion due to weak ICP effects. Separation occurred at 10% wt and markedly improved at 20% wt with a SR of ~1.3. For concentrations over 20% wt, Nafion precipitated out of the solution, and it was not suitable for patterning in nitrocellulose paper.

Figure 3 shows the characterization of separation parameters for the paper-based ICP device using FITC and calcein tracers as model analytes. There is good agreement between the experimental measurements and an analytical model[44] (see Supporting Information for analytical modeling of the separation process). As plotted in Figure 3a, SR improved with increasing voltage up to 140 V. Similarly, SR improved for higher channel aspect ratios, when (1) channel length increased with constant channel width and (2) channel width decreased with constant channel length (Figure 3b). As with capillary electrophoresis,[45] longer and narrower channels provide better separation performance. With regard to residence time, SR continuously improved up to 180 s and plateaued thereafter (Figure 3c). Band broadening becomes more significant after 180 s due to increased Joule heating, reducing any gain in peak-to-peak distance (as shown by the inset images in Figure 3c). While these operating parameters may change based on the application, the trend would be similar and equally predictable using the analytical expressions derived here (see the Supporting Information).

PCR-Free Hepatitis B Analysis. Workflows for both conventional and paper-based ICP DNA analysis are shown in Figure 4a. The infrastructure-intensive nature of PCR and gel electrophoresis is a major barrier to widespread DNA testing in both developed and developing regions.[46] As an alternative to increasing viral load through PCR thermal cycling, the device leverages ICP preconcentration to intensify the signal of target sequences prior to separation. We demonstrate this process using HBV DNA, a hepadnavirus with a genome consisting of circular, partially double-stranded DNA (dsDNA) of ~3200 base pairs (bp).[47]

Figure 4b shows the separation of a DNA standard containing dsDNA fragments from 100 bp to 2000 bp (6 fragments in total). The device had channel lengths of 7 mm and 10 mm (aspect ratios of 12 and 17, respectively), and mean pore diameters of 0.2 and 0.45 μm. The separations compare well to an ideal case in 2% agarose gel, where 3 of 6 fragments (the 2000/1200, 800, and 100 bp fragments) were resolved using the 7 mm channel devices and 4 of 6 fragments (the 2000/1200, 800, 400/200, and 100 bp fragments) using the10 mm channel devices, for both mean pore diameters (Figure 4, panels b and c). The devices were unable to resolve separate bands for the 2000 bp and 1200 bp fragments and the 400 bp and 200 bp fragments. However, the 2000/1200 bp and 400/200 bp fragments align with the 2000 bp and 400 bp positions in the 2% gel (best alignment achieved with the 10 mm channel device with 0.2 μm pore diameter) and can be used to mark these positions in the paper-based ICP device. The quality of each separation was quantified by the SR for the 2000/1200 bp and 800 bp fragments using the intensity profiles in Figure 4c. The SR values were comparable between all four separations, ranging from 0.5 to 0.7, with the highest resolution achieved

DOI: 10.1021/jacs.5b08523
J. Am. Chem. Soc. 2015, 137, 13913−13919

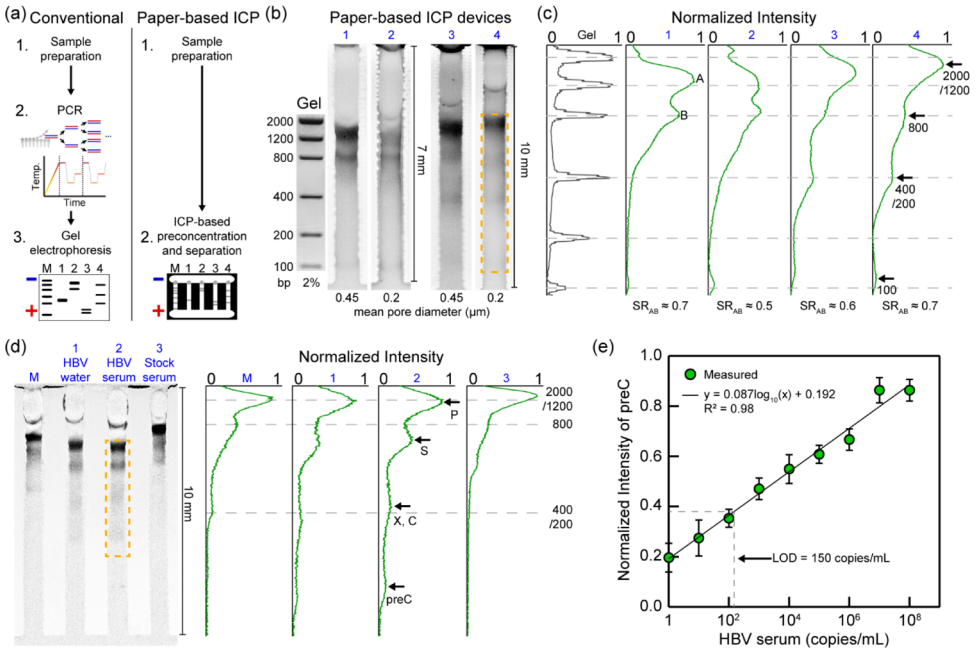

Figure 4. PCR-free hepatitis B analysis. (a) Comparison of conventional and paper-based ICP approaches for HBV DNA analysis. (b) Separation of a DNA standard containing dsDNA fragments ranging from 100 to 2000 bp (6 fragments in total), using 7 and 10 mm channel devices of two different mean pore diameters, 0.2 and 0.45 μm. The separations are compared to an ideal case in 2% agarose gel (image from Invitrogen). (c) Intensity profiles are measured for the gel and the four paper-based ICP cases using the region of interest (ROI) outlined by the yellow dashed box in (b). (d) Multiplexed analysis of the DNA standard, HBV DNA in water, HBV DNA in serum, and stock serum in a multichannel device. The intensity profile for each channel is measured using the ROI box. (e) A limit of detection (LOD) of 150 copies/mL is achieved by measuring the peak intensity of the precore (preC) fragment at serially diluted HBV DNA concentrations in serum. The LOD is the HBV DNA concentration at three standard deviations from a base intensity of 0.20. Each data point is the mean of the normal fit to the intensity profile of the preC fragment, with error bars as one standard deviation. Images have been contrast adjusted for presentation (similarly in each case).

with the highest aspect ratio (10 mm channel) devices. Notably, the 0.2 μm nitrocellulose pore diameter correlates to the pore size of the recommended 2% agarose gel,[48] enabling separation of the DNA standard with resolution comparable to conventional gel electrophoresis as observed for the 10 mm channel, 0.2 μm pore diameter device. Similarly, the 0.45 μm pore diameter device is representative of a 1% agarose gel,[48] which is generally used to separate larger DNA fragments from 500 bp to 10000 bp. These results demonstrate that the paper-based ICP approach is a viable means to separate DNA.

HBV DNA fragments (i.e., precore, core, surface, X, and polymerase) were simultaneously preconcentrated, separated, and detected using a multichannel device (Figure 4d). Each channel contained a different sample: (M) the DNA standard molecular size marker; (1) HBV DNA in water (HBV water) as a positive control; (2) HBV DNA in serum (HBV serum) as the target; and (3) stock serum as a negative control. DNA fragments in HBV water and serum were resolved after 10 min (at 150 V/cm) (Movie 4). In comparing the intensity profile of HBV serum to that of the DNA standard in channel M, the polymerase fragment, surface, and precore fragments were resolved, having sizes of 2535, 678, and 87 bp,[49] respectively. The X and core fragments, which have sizes of 463 and 555 bp, respectively,[49] were resolved from the other fragments as a combined band near the 400/200 bp mark. These results indicate that the device, in its current design, cannot be used to distinctly identify the X and core regions of the HBV genome for diagnosing hepatitis B. However, it can be used to reliably detect the surface and precore regions, which are routinely used for PCR-based HBV detection.[50,51] Importantly, the separation produced a distinct profile for the HBV serum, which corresponds to the profile for HBV water (i.e., positive control) in both position and intensity. A 100-fold increase in the signal of the precore fragment was achieved following preconcentration and separation. The stock serum produced a relatively high fluorescence signal, as a result of PicoGreen (the DNA stain employed here) binding to serum proteins in the absence of DNA.[52] When DNA was present, however, PicoGreen preferentially bound to the DNA, and the background fluorescence from serum proteins was less significant.[52] Collectively, these results demonstrate that paper-based ICP is amenable to multiplexed analysis and to amplified detection of target DNA in relevant biological fluids.

The early detection of acute HBV infection requires detection of low levels of HBV DNA (10^2 to 10^4 copies/mL[53]), generally necessitating PCR amplification. Such levels are present in serum after 4 weeks of infection, which is ~3 weeks prior to levels of serological markers (e.g., hepatitis B surface antigen) becoming detectable with immunoassays.[53] To evaluate the potential for early detection of HBV using the device, we determined its LOD for HBV DNA in serum by measuring the intensity of the precore fragment at different HBV DNA concentrations. The results in Figure 4e show a LOD of 150 copies/mL, applicable to early detection of acute HBV infection. This low LOD was achieved without prior PCR amplification and is comparable to that of commercial PCR systems (e.g., COBAS AMPLICOR Analyzer) with a LOD of 50−100 copies/mL. In addition to early detection, the paper-based ICP device has potential to monitor chronic HBV infection. During HBV chronicity, viral load typically ranges from 10^3 to 10^5 copies/mL and represents active viral replication.[47] With a LOD of 150 copies/mL and a dynamic

DOI: 10.1021/jacs.5b08523
J. Am. Chem. Soc. 2015, 137, 13913−13919

range up to 10^8 copies/mL, the device has potential to monitor HBV chronicity and evaluate antiviral therapies in real-time. Collectively, paper-based ICP enables low cost (materials cost <1 USD per test) and rapid (~10 min) HBV DNA analysis, with comparable performance to laboratory-based testing.

Clinical Assessment of Human Sperm DNA Integrity. Workflows for both conventional flow cytometry-based SCSA and the paper-based ICP approach are shown in Figure 5a. SCSA measures the proportion of sperm cells (typically 5000 to 10000 sperm are evaluated) with DNA denaturation, and the results are expressed as percent DNA Fragmentation Index or % DFI.[4] A low % DFI predicts higher success rates in natural/assisted reproduction and lower risks of transmission of genetic defects to the offspring.[54,55] The high capital and operating costs of flow cytometry are, however, barriers to widespread sperm DNA integrity assessment in both developed and developing regions.

As an alternative to SCSA, paper-based ICP devices were used to directly quantify % DFI of sperm cells in raw semen samples from patients and donors (n = 7; P1 to P4 and D1 to D3, respectively) at the Royal Victoria Hospital in Montreal, Canada. Specifically, single-stranded DNA (ssDNA) and dsDNA from lysed sperm cells were preconcentrated and separated over 15 min at 150 V/cm (a representative image is shown for P1 in Figure 5a). Intact and heavier dsDNA are concentrated at the depletion boundary, while fragmented and lighter ssDNA are concentrated further downstream. The intensity profile for this separation is plotted in Figure 5b, showing the overlapping ssDNA and dsDNA distributions, with SR calculated as ~0.5. The areas under the ssDNA and dsDNA normal fits were used to calculate % DFI (i.e., ssDNA area over the sum of ssDNA and dsDNA areas). It is possible that short dsDNA is present in the sample, and contributes to the overlap region between the two distributions. Short dsDNA, however, is not a significant third subpopulation here, given the quality of the fit of the two overlapped distributions and the observed profile.

SCSA distinguishes only dsDNA and ssDNA (not short dsDNA),[56] and results for both the clinical and paper-based ICP methods with both patient and donor samples are shown in Figure 5c. The device % DFI results strongly correlate (R^2 = 0.98) with those of SCSA for values ranging from 4% to 97%. In the clinic, a value greater than 30% indicates poor male fertility potential and a recommendation for assisted reproduction technologies (ART).[55] Here, P1 and P4 would be recommended for ART based on both the paper-based ICP and SCSA results, while P2, P3, and all donor samples show suitable fertility potential. Collectively, these results demonstrate the paper-based ICP approach as a promising method for scalable male fertility testing.

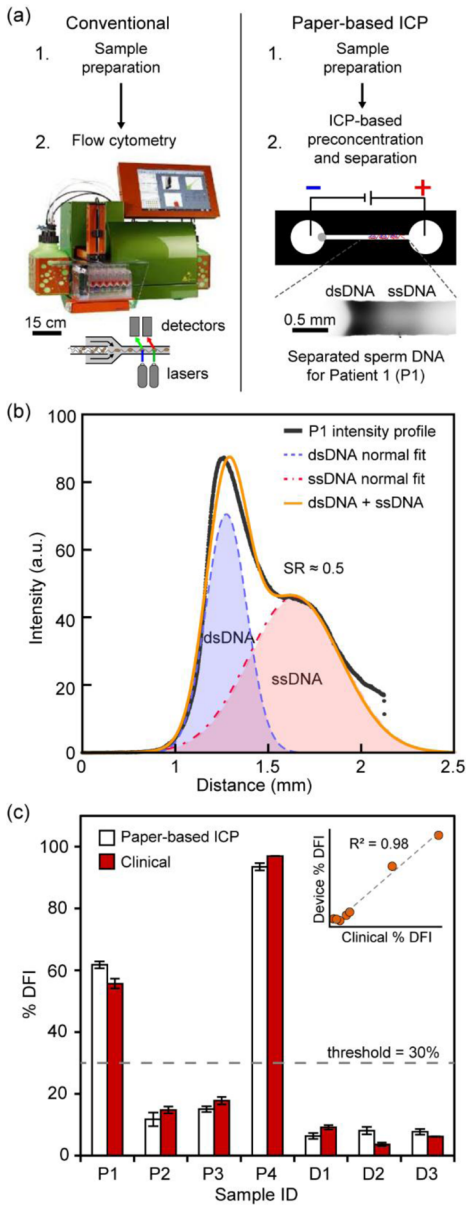

Figure 5. Clinical assessment of human sperm DNA integrity. (a) Comparison of conventional and paper-based ICP approaches. Contrast adjusted image showing preconcentration and separation of sperm DNA for patient P1. (b) Intensity profile of the separated DNA. The percent DNA Fragmentation Index (% DFI) is calculated using areas under the normal fits. (c) % DFI results for patients and donors. Inset shows correlation (R^2 = 0.98) between paper-based ICP and clinical results. A % DFI threshold of 30% is used to determine clinical outcome. Error bars for the device results represent one standard deviation of the normal fits. Clinical results are the average of two measurements with error bars as one standard deviation.

CONCLUSION

We demonstrated direct DNA analysis by leveraging electrokinetic transport at the interface of patterned nanoporous membranes in nitrocellulose paper. Paper-based ICP devices were used to detect HBV DNA in human serum and assess sperm DNA integrity in raw human semen, with comparable performance to the conventional gold standards. For hepatitis B testing, a LOD of 150 copies/mL was achieved with no prior viral load amplification, sufficient for early diagnosis of HBV. Multiplexed analysis of HBV was also demonstrated in a four-channel device. For male fertility assessment, the % DFI results from the paper-based ICP devices strongly correlated (R^2 = 0.98) with those of flow cytometry-based SCSA, providing identical clinical outcomes for tested patients and donors. Paper-based ICP enables inexpensive (materials cost <1 USD per test) and rapid (~10 min) DNA analysis in a simple format with potential for widespread application.

DOI: 10.1021/jacs.5b08523
J. Am. Chem. Soc. 2015, 137, 13913−13919

■ ASSOCIATED CONTENT

Supporting Information

The Supporting Information is available free of charge on the ACS Publications website at DOI: 10.1021/jacs.5b08523.

Analytical modeling of the separation process. (PDF)
Movie of Mode 1: transport without ICP (MPG)
Movie of Mode 2: preconcentration and separation with switching-polarity ICP (MPG)
Movie of Mode 3: direct preconcentration and separation with ICP (MPG)
Movie of Hepatitis B virus DNA analysis: direct preconcentration and separation (mode 3) in a four-channel device (MPG)

■ AUTHOR INFORMATION

Corresponding Author

*sinton@mie.utoronto.ca.

Notes

The authors declare no competing financial interest.

■ ACKNOWLEDGMENTS

The authors gratefully acknowledge an Alexander Graham Bell Canada Graduate Scholarship-Doctoral (CGS-D) from the Natural Sciences and Engineering Research Council of Canada (NSERC) to M.M.G. and an Ontario Graduate Scholarship (OGS) to R.N. The work was also enabled by funding from the NSERC Idea to Innovation Program and the Canadian Institutes of Health Research. Infrastructure funding from Canada Foundation for Innovation and the Ontario Research Fund (CFI and ORF) as well as ongoing program support through the NSERC Discovery Grant Program were also essential for this work.

■ REFERENCES

(1) Jobling, M. A.; Gill, P. *Nat. Rev. Genet.* **2004**, *5*, 739.
(2) Katsanis, S. H.; Katsanis, N. *Nat. Rev. Genet.* **2013**, *14*, 415.
(3) Tang, Y. W.; Procop, G. W.; Persing, D. H. *Clin. Chem.* **1997**, *43*, 2021.
(4) Evenson, D. P. In *Spermatogenesis: Methods and Protocols*; Carrell, D. T., Aston, K. I., Eds.; Methods in Molecular Biology; Humana Press: New York, 2013; Vol. 927, pp 147−164.
(5) Kelley, S. O.; Mirkin, C. A.; Walt, D. R.; Ismagilov, R. F.; Toner, M.; Sargent, E. H. *Nat. Nanotechnol.* **2014**, *9*, 969.
(6) Roy, S.; Chen, X.; Li, M.-H.; Peng, Y.; Anariba, F.; Gao, Z. *J. Am. Chem. Soc.* **2009**, *131*, 12211.
(7) Venkatesan, B. M.; Bashir, R. *Nat. Nanotechnol.* **2011**, *6*, 615.
(8) Brolo, A. *Nat. Photonics* **2012**, *6*, 709.
(9) Anker, J. N.; Hall, W. P.; Lyandres, O.; Shah, N. C.; Zhao, J.; Van Duyne, R. P. *Nat. Mater.* **2008**, *7*, 442.
(10) Chen, J. I. L.; Chen, Y.; Ginger, D. S. *J. Am. Chem. Soc.* **2010**, *132* (28), 9600.
(11) Kwon, S. J.; Bard, A. J. *J. Am. Chem. Soc.* **2012**, *134*, 10777.
(12) Gasparac, R.; Taft, B. J.; Lapierre-Devlin, M. A.; Lazareck, A. D.; Xu, J. M.; Kelley, S. O. *J. Am. Chem. Soc.* **2004**, *126*, 12270.
(13) Soleymani, L.; Fang, Z.; Sargent, E. H.; Kelley, S. O. *Nat. Nanotechnol.* **2009**, *4*, 844.
(14) Patolsky, F.; Zheng, G.; Lieber, C. M. *Nanomedicine* **2006**, *1*, 51.
(15) Weizmann, Y.; Chenoweth, D. M.; Swager, T. M. *J. Am. Chem. Soc.* **2011**, *133*, 3238.
(16) Martinez, A. W.; Phillips, S. T.; Whitesides, G. M.; Carrilho, E. *Anal. Chem.* **2010**, *82*, 3.
(17) Sackmann, E. K.; Fulton, A. L.; Beebe, D. J. *Nature* **2014**, *507*, 181.
(18) Cate, D. M.; Adkins, J. A.; Mettakoonpitak, J.; Henry, C. S. *Anal. Chem.* **2015**, *87*, 19.
(19) Gong, M. M.; Zhang, P.; MacDonald, B. D.; Sinton, D. *Anal. Chem.* **2014**, *86*, 8090.
(20) Renault, C.; Anderson, M. J.; Crooks, R. M. *J. Am. Chem. Soc.* **2014**, *136*, 4616.
(21) Yang, R.-J.; Pu, H.-H.; Wang, H.-L. *Biomicrofluidics* **2015**, *9*, 014122.
(22) Byrnes, S. A.; Bishop, J. D.; Lafleur, L.; Buser, J.; Lutz, B.; Yager, P. *Lab Chip* **2015**, *15*, 2647.
(23) Parolo, C.; Merkoçi, A. *Chem. Soc. Rev.* **2013**, *42*, 450.
(24) Yu, W. W.; White, I. M. *Anal. Chem.* **2010**, *82*, 9626.
(25) Yu, W. W.; White, I. M. *Analyst* **2013**, *138*, 1020.
(26) Liu, Q.; Wang, J.; Wang, B.; Li, Z.; Huang, H.; Li, C.; Yu, X.; Chu, P. K. *Biosens. Bioelectron.* **2014**, *54*, 128.
(27) Kumar, S.; Kaushik, S.; Pratap, R.; Raghavan, S. *ACS Appl. Mater. Interfaces* **2015**, *7*, 2189.
(28) Höltzel, A.; Tallarek, U. *J. Sep. Sci.* **2007**, *30*, 1398.
(29) Kim, S. J.; Ko, S. H.; Kang, K. H.; Han, J. *Nat. Nanotechnol.* **2010**, *5*, 297.
(30) MacDonald, B. D.; Gong, M. M.; Zhang, P.; Sinton, D. *Lab Chip* **2014**, *14*, 681.
(31) Scarff, B.; Escobedo, C.; Sinton, D. *Lab Chip* **2011**, *11*, 1102.
(32) Moghadam, B. Y.; Connelly, K. T.; Posner, J. D. *Anal. Chem.* **2014**, *86*, 5829.
(33) Moghadam, B. Y.; Connelly, K. T.; Posner, J. D. *Anal. Chem.* **2015**, *87*, 1009.
(34) Rosenfeld, T.; Bercovici, M. *Lab Chip* **2014**, *14*, 4465.
(35) Li, X.; Luo, L.; Crooks, R. M. *Lab Chip* **2015**, *15*, 4090.
(36) Ge, L.; Wang, S.; Ge, S.; Yu, J.; Yan, M.; Li, N.; Huang, J. *Chem. Commun.* **2014**, *50*, 5699.
(37) Chen, S.-S.; Hu, C.-W.; Yu, I.-F.; Liao, Y.-C.; Yang, J.-T. *Lab Chip* **2014**, *14*, 2124.
(38) Luo, L.; Li, X.; Crooks, R. M. *Anal. Chem.* **2014**, *86*, 12390.
(39) Fridley, G. E.; Holstein, C. A.; Oza, S. B.; Yager, P. *MRS Bull.* **2013**, *38*, 326.
(40) Zangle, T. A.; Mani, A.; Santiago, J. G. *Chem. Soc. Rev.* **2010**, *39*, 1014.
(41) Thormann, W.; Zhang, C. X.; Caslavska, J.; Gebauer, P.; Mosher, R. A. *Anal. Chem.* **1998**, *70*, 549.
(42) Giddings, J. C. *Unified Separation Science*; John Wiley & Sons Inc.: Hoboken, 1991.
(43) Kim, M.; Jia, M.; Kim, T. *Analyst* **2013**, *138*, 1370.
(44) Jorgenson, J. W.; Lukacs, K. D. *Anal. Chem.* **1981**, *53*, 1298.
(45) Bharadwaj, R.; Santiago, J. G.; Mohammadi, B. *Electrophoresis* **2002**, *23*, 2729.
(46) Yager, P.; Domingo, G. J.; Gerdes, J. *Annu. Rev. Biomed. Eng.* **2008**, *10*, 107.
(47) Ganem, D.; Prince, A. M. *N. Engl. J. Med.* **2004**, *350*, 1118.
(48) Narayanan, J.; Xiong, J.-Y.; Liu, X.-Y. *J. Phys.: Conf. Ser.* **2006**, *28*, 83.
(49) Norder, H.; Couroucé, A. M.; Magnius, L. O. *Virology* **1994**, *198*, 489.
(50) Gerken, G.; Gomes, J.; Lampertico, P.; Colombo, M.; Rothaar, T.; Trippler, M.; Colucci, G. *J. Virol. Methods* **1998**, *74*, 155.
(51) Weinberger, K. M.; Wiedenmann, E.; Böhm, S.; Jilg, W. *J. Virol. Methods* **2000**, *85*, 75.
(52) Chen, J. A.; Meister, S.; Urbonaviciute, V.; Rödel, F.; Wilhelm, S.; Kalden, J. R.; Manger, K.; Voll, R. E. *Autoimmunity* **2007**, *40*, 307.
(53) Rehermann, B.; Nascimbeni, M. *Nat. Rev. Immunol.* **2005**, *5*, 215.
(54) Zini, A.; Boman, J. M.; Belzile, E.; Ciampi, A. *Hum. Reprod.* **2008**, *23*, 2663.
(55) Zini, A. *Syst. Biol. Reprod. Med.* **2011**, *57*, 78.
(56) Evenson, D.; Jost, L. *Methods Cell Sci.* **2000**, *22*, 169.

DOI: 10.1021/jacs.5b08523
J. Am. Chem. Soc. 2015, 137, 13913−13919